First-Passage Processes in the Genome

Yaojun Zhang[1,2] and Olga K. Dudko[1]

[1]Department of Physics, University of California at San Diego, La Jolla, California 92093; email: dudko@physics.ucsd.edu

[2]Princeton Center for Theoretical Science, Princeton University, Princeton, New Jersey 08544

Annu. Rev. Biophys. 2016. 45:117–34

The *Annual Review of Biophysics* is online at biophys.annualreviews.org

This article's doi: 10.1146/annurev-biophys-062215-010925

Keywords

first-passage time, genomic interaction, viscoelasticity, fractional Langevin motion

Abstract

Many essential processes in biology share a common fundamental step—establishing physical contact between distant segments of DNA. How fast this step is accomplished sets the "speed limit" for the larger-scale processes it enables, whether the process is antibody production by the immune system or tissue differentiation in a developing embryo. This naturally leads us to ask, How long does it take for DNA segments that are strung out over millions of base pairs along the chromatin fiber to find each other in the crowded cell? This question, fundamental to biology, can be recognized as the physics problem of the first-passage time, or the waiting time for the first encounter. Here, we review a number of approaches to revealing the physical principles by which cells solve, with astonishing efficiency, the first-passage problem for remote genomic interactions.

Contents

THE CHALLENGE: IN A CROWD AND PRESSED FOR TIME, DISTANT PARTS OF DNA MUST FIND EACH OTHER

Many processes in biology rely on the ability of remote DNA segments to find each other within the cell nucleus. Separated by thousands to millions of base pairs along the DNA, the segments must establish contact quickly enough to ensure that the larger-scale cellular processes are completed on time. The segments in this rather busy scenario may, for example, represent an enhancer and its target promoter, which must find each other in order to activate gene expression (7, 27). This scenario also arises during packing of chromatin, when distant chromatin segments must come into physical proximity to be clamped by proteins and packaged into bundles of loops (8, 46). Yet in another setting, encounters between distant DNA segments, followed by genetic recombination, are responsible for the production of a virtually unlimited number of antibodies by our white blood cells (1, 48). How long does it take for two DNA segments, located millions of base pairs apart, to encounter each other in the crowded interior of the nucleus (**Figure 1**)? This question, originating from diverse and fascinating living phenomena, has its counterpart in physics, where it is known as the first-passage time problem, or the problem of a stochastic variable reaching a specified value for

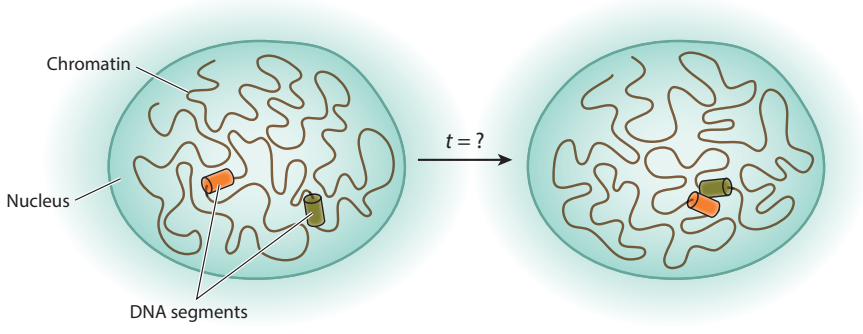

Figure 1

A genomic event in which distant parts of chromosomal DNA have to find each other—and have to do so in a timely fashion—is a precursor to a wide range of essential processes of life. This review discusses a variety of approaches to revealing the physical principles that enable cells to efficiently solve the first-passage time problem for its genome.

the first time (41). Pulling on the threads of the first-passage time problem for genomic segments unravels further questions. How does DNA move? What is the role of nuclear environment in this motion? What is the key to rapid rates of encounters between distant genomic elements? This review discusses the physical principles by which cells solve the first-passage problem for remote genomic interactions with astonishing efficiency (**Figure 1**).

The natural setting in which genomic interactions take place—the interior of the nucleus—is ordered and crowded, yet dynamic. The order has been revealed with the help of advanced techniques, which have identified multiple levels of hierarchy in the way the genome is compacted—from chromatin fibers to loops to domains and territories (13, 17, 30). The second property, crowdedness, has become apparent in its full extent upon realization that not only is the genome highly compacted but also surrounded by macromolecules with intermolecular spacing comparable to the size of the macromolecules themselves (39). The third, dynamic aspect is ultimately what brings all the pieces together to make genomic interactions happen. Then, how does the genome move? The characteristic dimensions of chromatin—on the order of ten nanometers in thickness—are small enough for thermal fluctuations to have palpable effects on its motion. It is therefore appropriate to think about chromatin motion as diffusion, or Brownian motion resulting from random collisions of the chromatin elements with the molecules of the nucleus. In the absence of evidence for sophisticated active mechanisms of delivering DNA segments to their remote counterparts, diffusion emerges as a likely dominant means of transport underlying remote DNA encounters. If so, this means that, in the course of random motion, distant chromosomal segments must end up, by chance, in the same place at the same time—and in a sufficiently short amount of time. How probable is such an outcome? What determines its probability? We review several plausible scenarios of random motion of genomic elements and examine the efficiency of such motion for genomic interactions in the face of the multilevel packing and crowding.

To formulate a quantitative description of genomic motion and interactions in the nucleus, we must establish the dominant mechanism(s) of this motion. Indeed, the mechanism determines the choice of the appropriate physical model, which, in turn, provides the framework for the quantitative description we are seeking. How can we identify the dominant mechanism on the basis of the observed DNA trajectories? We illustrate the power of quantitative diagnostic tools that can help reveal the type of diffusive motion, assess ergodicity (i.e., the equivalence of an average over trajectories and an average over time), and probe the degree of correlation of motion in time and space (32, 50). Putting together all of the pieces extracted from DNA trajectories can help us recognize the dominant mechanism of motion.

In the theoretical physics tradition, we aim at a theory that is reasonably simple to serve as a guide for intuition and yet (*a*) captures the general principles, (*b*) explains observations, and (*c*) generates testable predictions. In this regard, once the physical mechanism of DNA motion in the nucleus has been established, one can attempt to abstract the motion with a physical model. We review a number of potentially relevant models, each emphasizing a particular aspect of motion. The model thought to be most appropriate, complemented by the parameters extracted from experiment, provides the framework for computer simulations of the DNA motion in the nucleus. The model also serves as a basis for predictive analytical relationships regarding the first-passage times for genomic interactions. The predictions from the theory can help design future studies that could reveal the principles of the spatiotemporal organization of the genome.

THE GEOMETRY OF GENOME PACKING AND THE HIERARCHY OF GENOME MOTIONS

The motion of genomic segments and, hence, the likelihood of their mutual encounters are strongly influenced by the way the genome is organized in the nucleus. Conversely, the genome

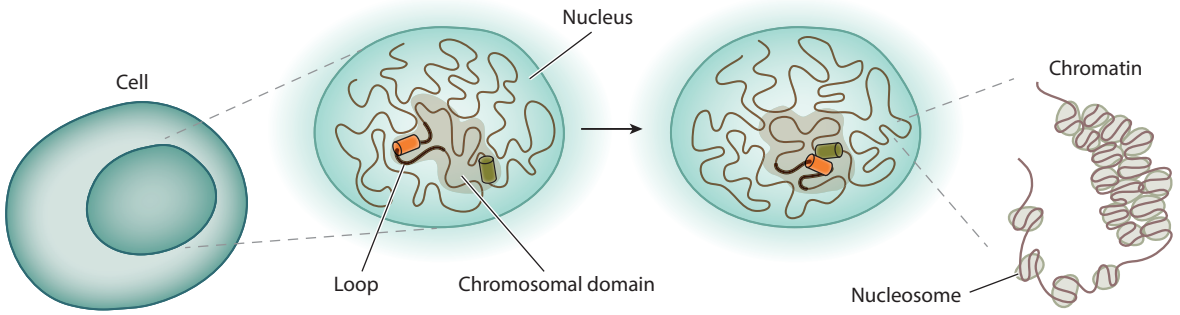

Figure 2

Motion and interactions of genomic segments are strongly affected by the genome architecture. Interphase chromatin is folded into loops, which are further compacted into chromosomal domains. Genomic interactions mostly occur within the same domain.

architecture itself is a result of the motion of DNA and other macromolecules. To better appreciate the link between DNA motion and structure, it is useful to review the fundamentals of genome organization.

The DNA of a eukaryotic cell is tightly compacted, yet it is folded in a way that makes it accessible for the replication, repair, and gene expression machinery of the cell. At the first level of compacting, DNA forms complexes, called nucleosomes, with proteins. Nucleosomes are further packed into chromatin fibers (**Figure 2**). The nature of packing at subsequent levels in the hierarchy depends on the phase of the cell cycle. The structure of chromosomes during interphase—the stages of the cell cycle when the cell is actively transcribing its genes and when productive genomic interactions take place—is of particular interest to researchers. Yet interphase is the time when such details are least visible because of the decondensed state of the chromosomes. Nevertheless, experimental techniques such as fluorescent labeling and chromosome conformation capture have revealed some striking details of the global structure of the interphase chromosomes. Contrary to earlier views of the interphase chromatin as being randomly distributed within the nucleus like a bowl of spaghetti, multiple levels of chromatin organization have been discovered (**Figure 2**) (6, 12, 13, 15, 17, 30). The chromatin is folded into bundles of loops, known as topological association domains (TADs), which are composed of thousands to millions of base pairs. Despite being relatively decondensed, interphase chromosomes occupy discrete territories with no extensive intertwining. The entire chromatin network is immersed in nucleoplasm, a highly viscous nuclear liquid crowded with macromolecules (1).

This hierarchical structure of the genome is also highly dynamic, exhibiting a hierarchy of motions at various spatial and temporal scales (28, 45, 52):

1. Thermal fluctuations, or random collisions with the surrounding molecules, have a profound effect on the motion of DNA segments owing to their small, nanometer-scale dimensions. The segments are also subject to active fluctuations and biased motion driven by motor proteins.
2. Thermal motion of DNA segments is likely to be interspersed with pauses as a result of binding to other molecules. The motion may also be obstructed by hard-wall-like objects, such as organelles and nuclear lamina. Thermal motion of the segments takes place concurrently with back-and-forth bouncing against springy semiflexible elements such as chromatin fibers and proteins (32, 50).
3. DNA motion is altered by changes in the basic chromatin structure, such as the unfolding of the chromatin fiber into a more flexible configuration during active transcription (21).

4. DNA motion is restricted by higher-order structural elements—loops, domains, and territories.
5. These structural elements are themselves dynamic: Loops can form and open repeatedly (2), domains can merge in the course of cell development (25), and chromosomal territories can move relative to each other over several micrometers on a timescale of hours (54).
6. Genomic motions at various levels are superimposed with translational and rotational motion of the nucleus and the cell as a whole.

The hierarchical and dynamic organization of DNA is not unique to eukaryotes. Although prokaryotic cells lack a defined nucleus, multiple levels of organization, including loops and domains, as well as dynamic behavior, have been found in the nucleoid, the chromosome of prokaryotes (20, 36, 47).

DNA MOTION IDEALIZED: CANDIDATE MODELS

In order to interpret quantitative observations of genomic motion and to make quantitative predictions regarding genomic interactions, a quantitative model is required. Below, we discuss a suite of candidate physical models, each emphasizing a particular aspect of DNA motion. We examine the predictions of these models regarding an important characteristic of motion—the mean squared displacement (MSD). MSD can be thought of as a measure of the effective space explored by the random walker during the time elapsed.

We preface our overview of candidate models with two basic observations regarding DNA motion. First, a segment of DNA is a monomer in a polymer chain, meaning that, unlike a free particle, it experiences restoring forces from the neighboring monomers as it moves (**Figure 3**). Second, the highly crowded environment in which DNA motion takes place is likely to make the motion drastically different from that of a polymer in a diluted solution. To dissect the effects of each of these factors—the polymer nature of DNA itself and the crowded environment in which it moves—we begin by reviewing classical models of polymer dynamics (**Figure 4**) and then discuss several approaches to modeling diffusive motion in a crowded environment (**Figure 5**).

A chain of beads that are connected by harmonic springs (**Figure 4*a***) is the picture of a polymer in the Rouse model (18, 42), where each bead represents a polymer segment. The time evolution of the position, $\boldsymbol{R}_n(t)$, of the nth bead (out of total N beads) undergoing Brownian motion can be

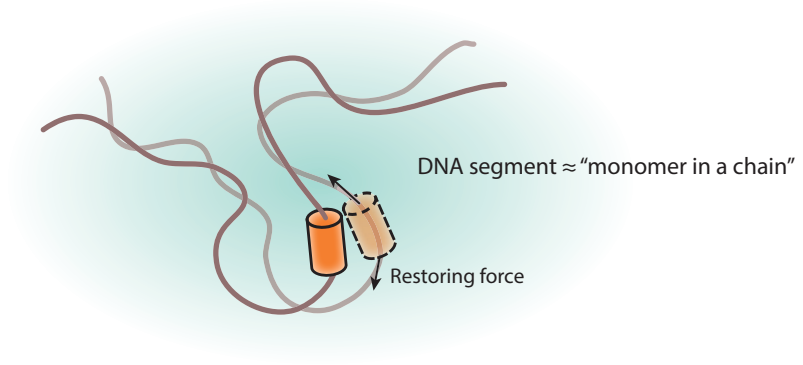

Figure 3

Unlike the case of a free particle, any movement of a DNA segment results in restoring forces on this segment exerted by the neighboring segments of the chain.

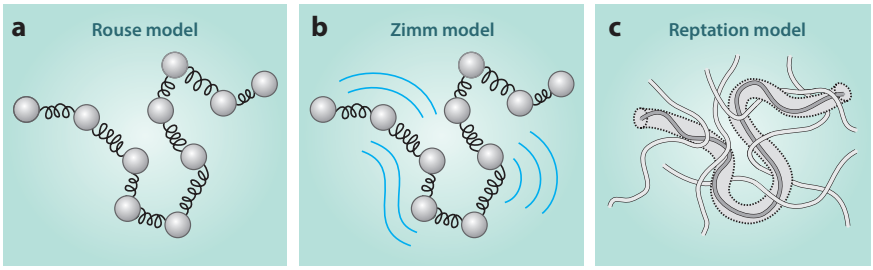

Figure 4

Different ways of idealizing the polymer dynamics. (*a*) The Rouse model views a polymer as a so-called ideal chain, or a set of beads connected by harmonic springs; each bead is subject to a random thermal force and a drag force. (*b*) The Zimm model extends the Rouse model by including hydrodynamic interactions, mediated by the solvent, between different parts of the chain. (*c*) The reptation model describes thermal motion of a long chain slithering through an effective tube formed by a concentrated solution of interpenetrating chains, resembling an entangled collection of snakes.

described by the overdamped (i.e., with inertia effects neglected) Langevin equation

$$\frac{d\boldsymbol{R}_n}{dt} = \frac{1}{\gamma}[-k(2\boldsymbol{R}_n - \boldsymbol{R}_{n+1} - \boldsymbol{R}_{n-1}) + \boldsymbol{F}_n + \boldsymbol{f}_n]. \quad 1.$$

The friction constant, γ, characterizes the viscous properties of the solution. The flexibility of the polymer is described by the spring constant $k = \frac{3k_BT}{b^2}$, in which b is the Kuhn length (approximately equal to twice the persistent length, or the length over which the polymer is roughly straight), and k_B is the Boltzmann constant. The fact that the spring constant is proportional to temperature T reflects the entropic nature of the polymer "spring." Through the external force term, F_n, the Rouse model can be generalized to include, for example, the effects of structural elements confining the motion or molecular motors providing active transport. The random force $\boldsymbol{f}_n$ describes the collisions of the bead with the surrounding molecules in the solution. This force has a Gaussian distribution with zero mean and with the variance given by $\langle f_{ni}(t) f_{mj}(t')\rangle = 2\gamma k_B T \delta_{nm}\delta_{ij}\delta(t-t')$, where $i, j \in \{x, y, z\}$ denote the components of $\boldsymbol{f}_n$. In the expression for the variance, which is also known as the fluctuation-dissipation theorem, the only nonzero terms are those with $n = m$ (i.e., for

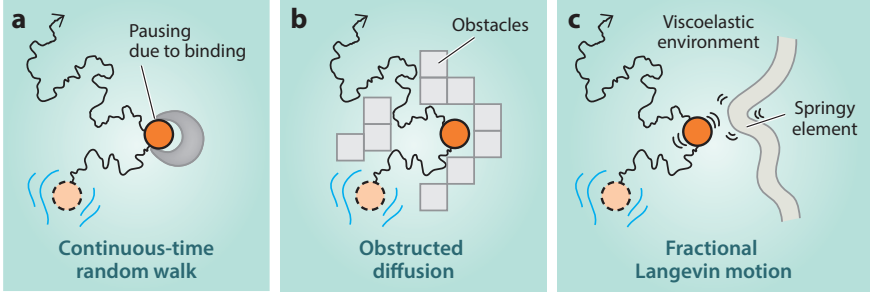

Figure 5

Diffusive motion of a particle in different types of the crowded environment. (*a*) The continuous-time random walk model describes diffusive motion interspersed by pauses resulting from binding events. (*b*) The obstructed diffusion model describes the motion of a particle in a high concentration of hard-wall-like obstacles. (*c*) The fractional Langevin motion model describes the thermal motion of a particle that bounces back and forth against a springy network.

the same bead) and $i = j$ (i.e., along the same spatial direction), reflecting the uncorrelated nature of the noise in the Langevin equation, Equation 1. In the absence of an external force, the MSD of a segment (a bead) undergoing three-dimensional (3D) motion scales with the elapsed time τ as $6D\tau^{0.5}$ for times $\tau < \tau_{\rm rot}$. Here, $D = b\sqrt{k_B T/(3\pi\gamma)}$ is the anomalous diffusion coefficient and $\tau_{\rm rot} = \gamma N^2 b^2/(3\pi^2 k_B T)$ is the longest relaxation timescale of the chain dynamics, corresponding to rotational motion (18, 42, 50). Note that the MSD of the segment grows more slowly with the elapsed time than it would for normal diffusion; the motion of the segment is said to be subdiffusive. The decrease of the scaling exponent from 1 (as expected for normal diffusion) to 0.5 is due to the restoring forces exerted on the segment by its neighbors (**Figure 3**). We can use the above expressions to estimate D and $\tau_{\rm rot}$ for a chromatin segment: using the input values of 1 to 30 μm for the contour length, 40 to 200 nm for the persistence length of the fiber, 0.05 μm for the size of the segment, 0.01 kg $m^{-1}s^{-1}$ for the dynamic viscosity of nucleoplasm, and assuming room temperature, we obtain the range 0.01–0.1 $\mu m^2/s^{0.5}$ for the diffusion coefficient D and the range 0.1–100 s for the relaxation timescale $\tau_{\rm rot}$. The Rouse model of polymer dynamics is most suitable for situations in which the environmental effects of the entanglement and crowding, as well as hydrodynamic interactions, are negligible.

The Zimm model (18, 53) extends the Rouse model by including hydrodynamic effects from the surrounding medium. The basic picture is that the motion of some part of the chain causes hydrodynamic flow that, in turn, affects the motion of a distant part of the chain (**Figure 4*b***). The hydrodynamic interactions somewhat complicate the corresponding equation of motion, Equation 1, in which the scalar $1/\gamma$ is now replaced with a nondiagonal mobility matrix (18). The MSD of the chain segment scales with the elapsed time as $\sim\tau^{0.67}$ in Θ solvent (50, 53). Θ solvent is a solvent in which attractive and repulsive interactions between different parts of the chain cancel each other; as a result, the polymer itself behaves like an ideal chain. The increase of the scaling exponent from 0.5 in the Rouse model to 0.67 in the Zimm model is the consequence of the hydrodynamic interactions. The hydrodynamic flow caused by the motion of one segment tends to make other segments move in the same direction; this resulting movement, in turn, reinforces the motion of the original segment, weakening the subdiffusive effects. The Zimm model is most suitable for describing the dynamics of polymers in a dilute (i.e., with no crowding) solution with strong hydrodynamic effects.

The reptation model (14, 18) describes thermal motion of long, entangled chains slithering through one another in a concentrated polymer solution, resembling a ball of snakes (**Figure 4*c***). The confinement formed by the surrounding chains restricts the motion of the chain to sliding along the imaginary tube. At short times, when the entanglement effect is not yet significant, the dynamics of the segment are described by the familiar Rouse model, so that MSD $\sim\tau^{0.5}$. At longer times, the motion of the segment is dominated by the topological constraints of the entangled polymers, which slow the growth of the MSD of the segment with time: MSD $\sim\tau^{0.25}$ (14, 18, 50). The reptation model is best applicable to particular situations in which the polymer motion is constrained to sliding within the tube-like confinement created by the entangled polymers (**Figure 4*c***).

Recalling that the motion takes place in the nucleus, let us shift the focus from polymer dynamics to the effect of the crowded environment and begin with the simplest case of the thermal motion of a single particle. Consider a diffusing particle that pauses occasionally to interact with the binding partners it encounters (**Figure 5*a***). Such a diffusive motion interspersed with pauses is described by the continuous-time random walk (CTRW) model (35, 44). Mathematically, CTRW is built of a sequence of alternating jumping and waiting events with randomly distributed lengths of jumps and times of pausing. When the distribution of the pausing times is broad, with the tail described by a power law, $p(t) \sim t^{-(1+\alpha)}$ $(0 < \alpha < 1)$, but the distribution of jump lengths is ordinary

(i.e., with a finite variance), then the ensemble-averaged MSD of the particle scales with time as MSD $\sim \tau^{\alpha}$ ($0 < \alpha < 1$), as one would expect from subdiffusive motion. However, both the time-averaged MSD and the time-and-ensemble-averaged MSD grow linearly with time: MSD $\sim \tau$, just as in normal diffusion. The difference in behaviors of the particle when the motion is averaged over time and over the ensemble points to an important property of subdiffusive CTRW processes: broken ergodicity (22, 34).

Next, consider a particle navigating through a maze of macromolecules that act as immobile, hard obstacles (**Figure 5*b***). The resulting motion of the particle is described by the obstructed diffusion (OD) model (3, 43). The properties of the motion are determined by the density of the obstacles relative to the so-called critical threshold density, or the highest density at which the particle can still make its way through the obstructive medium. At the obstacle density below the critical threshold, the particle moves weakly-subdiffusively (i.e., with slight deviations from normal diffusion) at short times, and normal diffusion is recovered at long times. At the critical density, the motion is subdiffusive, with a constant scaling exponent, at all times: MSD $\sim \tau^{\alpha}$ ($0 < \alpha < 1, \alpha = const$). Above the critical density, the motion of the particle gets increasingly subdiffusive with time and eventually becomes confined at long times, with α approaching zero (3, 43).

Yet another type of crowded environment is a solution of semiflexible macromolecules. A particle moving through such an environment experiences both viscous and elastic effects, such that it not only diffuses but also bounces back and forth against the springy macromolecular network (**Figure 5*c***). The motion of the particle is captured by the fractional Langevin motion (FLM) model (26, 33). The corresponding equation of motion is

$$m\frac{d^2\boldsymbol{R}}{dt^2} = -\gamma \int_{-\infty}^{t} K(t-t')\frac{d\boldsymbol{R}(t')}{dt'}dt' + \boldsymbol{F} + \boldsymbol{f}. \qquad 2.$$

Equation 2, known as the fractional Langevin equation, possesses two features that distinguish it from the ordinary Langevin equation (Equation 3): the presence of a memory kernel, K, in the frictional force term and the correlated nature of the random force f describing thermal fluctuations. Specifically, the memory kernel is given by (23, 40)

$$K(t-t') = \frac{(2-\alpha)(1-\alpha)}{|t-t'|^{\alpha}} + \frac{2(2-\alpha)}{|t-t'|^{\alpha-1}}\delta(t-t'),$$

where α ($0 < \alpha < 1$) controls the rate of decay of the kernel at long times, $K(t) \sim t^{-\alpha}$. A curious property of Equation 2 is that the integral term with the memory kernel can be rewritten in the form of a fractional derivative—a likely origin of the term "fractional" in the name of Equation 2 (33). The random force f, which now contains temporal correlations, has a Gaussian distribution with zero mean and with the variance given by $\langle f_i(t) f_j(t')\rangle = \gamma k_B T \delta_{ij} K(t-t')$. In the special case of $\alpha = 1$, the fractional Langevin equation, Equation 2, reduces to the ordinary Langevin equation (29)

$$m\frac{d^2\boldsymbol{R}}{dt^2} = -\gamma\frac{d\boldsymbol{R}}{dt} + \boldsymbol{F} + \boldsymbol{f}. \qquad 3.$$

In the absence of external force $\boldsymbol{F}$, MSD of the fractional Langevin motion, governed by Equation 2, scales as MSD $\sim \tau^{\alpha}$ ($0 < \alpha < 1$) at all times outside the ballistic regime (the ballistic regime corresponds to an early stage of motion, $\tau \ll m/\gamma$, before collisions with the surrounding molecules have slowed the particle down and randomized its direction) (16, 23).

We considered several basic approaches to describing polymer dynamics (**Figure 4**) and diffusion in a crowded environment (**Figure 5**). Attempts to merge these aspects of DNA motion, as well as other factors reflecting the organization and dynamics of the genome, into a "complete

model" are likely to result in a model so overwhelmingly complex that it would hardly be of much use in guiding our intuition and deciphering general principles. Our task would become simpler if we knew the relative importance of these factors. The model could then focus on those aspects that dominate genomic motion. Useful hints as to what factors might dominate DNA motion can be obtained by taking a close look at the available experimental data. With proper analysis, the data may reveal certain characteristics of the underlying motion of DNA that would flag a particular dominant mechanism of motion. Several useful diagnostic tools for implementing such analysis are discussed in the following section.

HOW DOES DNA ACTUALLY MOVE? TOOLS FOR IDENTIFYING THE MECHANISM

Recent in vivo tracking experiments enabled the visualization of motion of individual segments of DNA in its native environment, the nucleus (9, 32, 50). These experiments report the trajectories—that is, the x, y, and z components of the position of the segment as a function of time t. Recorded from a relatively large number (hundreds to thousands) of cells, the trajectories contain information on both temporal and ensemble properties of motion. On the basis of the available trajectories, how can we identify the dominant mechanism that governs DNA motion?

The most straightforward tool for deciphering the properties of motion from the trajectories is the MSD (**Figure 6*a***). The ensemble-averaged MSD, defined as MSD $\equiv \langle (\boldsymbol{R}(\tau) - \boldsymbol{R}(0))^2 \rangle$, first computes the squared displacement for each particle during time τ and then determines the average (denoted as $\langle \ldots \rangle$) over the entire ensemble of particles. In a different approach, the

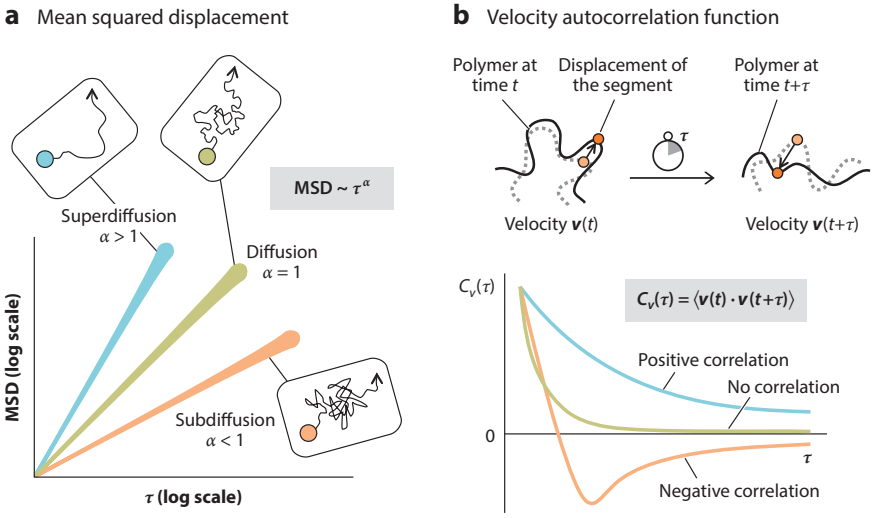

Figure 6

Quantitative tools for establishing the mechanism of motion from trajectories: (*a*) mean squared displacement (MSD) and (*b*) velocity autocorrelation function (VAF). MSD is a measure of the extent of excursions of the random walker during time τ. For many systems, MSD scales with the elapsed time as MSD$\sim\tau^{\alpha}$, resulting in a linear graph of slope α on a log-log plot. The scaling exponent α determines the type of diffusion (normal diffusion versus anomalous diffusion). The VAF, $C_v(\tau)$, indicates the degree to which the velocities of the particle are correlated when separated by time τ. Normal diffusion exhibits no correlations, whereas subdiffusion and superdiffusion lead to negative and positive correlations, respectively.

time-averaged MSD, which is defined as MSD $\equiv \lim_{T\to+\infty} \frac{1}{T}\int_0^T (\boldsymbol{R}(t+\tau)-\boldsymbol{R}(t))^2 dt$, computes the squared displacement of a single particle during time τ and averages the result (hence the integration) over a long period of time. Finally, the time-and-ensemble-averaged MSD is obtained by performing both types of averaging: MSD $\equiv \lim_{T\to+\infty} \frac{1}{T}\int_0^T \langle(\boldsymbol{R}(t+\tau)-\boldsymbol{R}(t))^2\rangle dt$. For a so-called ergodic process, the ensemble-averaged MSD must agree with the time-averaged MSD. For a diverse range of systems, MSD scales with the elapsed time as MSD $\sim \tau^\alpha$. On a log-log plot, this scaling results in a linear graph with slope α (**Figure 6*a***). The scaling exponent α determines the type of diffusion: $\alpha = 1$ corresponds to normal diffusion, whereas $\alpha \neq 1$ corresponds to anomalous diffusion. Specifically, at $\alpha > 1$, the particle undergoes superdiffusion, in which its trajectory appears less rugged than the trajectory in normal diffusion. At $\alpha < 1$, the motion is subdiffusive, marked by more rugged trajectories.

Another informative tool for deducing the dominant mechanism from the trajectories is the velocity autocorrelation function (VAF) (**Figure 6*b***). VAF describes the degree of correlation between the velocities of a particle at two time instants separated by the time interval τ. Mathematically, VAF is defined as $C_v(\tau) \equiv \langle \boldsymbol{v}(t)\cdot\boldsymbol{v}(t+\tau)\rangle$, where the dot product of two velocity vectors is averaged over time and/or ensemble. For normal diffusion, where the individual steps are uncorrelated, the corresponding VAF exhibits no correlations. In contrast, VAFs for subdiffusion and superdiffusion are marked by negative and positive correlations, respectively (**Figure 6*b***).

To illustrate the power of MSD and VAF as diagnostic tools, let us apply these concepts to the actual 3D trajectories of DNA segments recorded in live mammalian B cells (white blood cells whose primary function is to produce antibodies in response to antigens) (32) (**Figure 7**). Through analysis of the radial component of motion only, the rotational and translational motion of the nucleus and the cell as a whole can be decoupled from the motion we are interested in—that of the DNA itself (10, 32, 49). In the following, the radial components of displacement and velocity are used to compute MSD and VAF.

The time-averaged MSD computed for the individual trajectories and the ensemble-averaged MSD computed across all the trajectories are shown in **Figure 7*a*** as functions of the time lag τ on a log-log scale. A least-squares fit of the time-averaged MSD curves to the equation MSD $= 2D\tau^\alpha$ yields the anomalous diffusion coefficient $D = 0.001 - 0.005\ \mu m^2/s^{0.5}$ and the scaling exponent $\alpha = 0.42 \pm 0.25$. The corresponding fit of the ensemble-averaged MSD yields $D = 0.002\ \mu m^2/s^{0.5}$ and $\alpha = 0.52$. The observations that the scaling exponent is significantly smaller than 1 and that both time- and ensemble-averaged MSD are characterized by very similar diffusion coefficients and scaling exponents ($\alpha \approx 0.5$) lead to two important conclusions: DNA motion is subdiffusive, and the process of its motion is ergodic. Interestingly, similar values of α have been reported for DNA motion in other species: $\alpha = 0.51 \pm 0.20$ for the motion of telomeres in human cells (9); $\alpha = 0.41 - 0.47$ for the *GAL* locus motion in yeast (10); and $\alpha = 0.39 \pm 0.04$ for the 84′ locus motion in *E. coli* (50). The similarity of the values of the scaling exponent across species indicates that DNA motion in these systems is likely governed by a universal physical mechanism.

The VAFs computed from the DNA trajectories are shown in **Figure 7*b***. Each curve is calculated as $C_v^\delta(\tau) = \langle v(t+\tau)v(t)\rangle$ with τ being the time lag over which the correlation in velocities is examined. The velocities themselves are calculated directly from the trajectories according to the standard definition of the average velocity as the displacement over the time interval (δ) during which the displacement occurred: $v(t) = \frac{1}{\delta}(r(t+\delta) - r(t))$. A pronounced feature of the VAF curves for all values of δ is a dip into negative values—an indication of negative correlations in the DNA motion (see **Figure 6**). Furthermore, when the VAF curves corresponding to different values of δ are all plotted against a rescaled time lag, (τ/δ), they collapse onto a universal curve (**Figure 7*b***, bottom). The collapse is an indication that the motion of DNA segments possesses

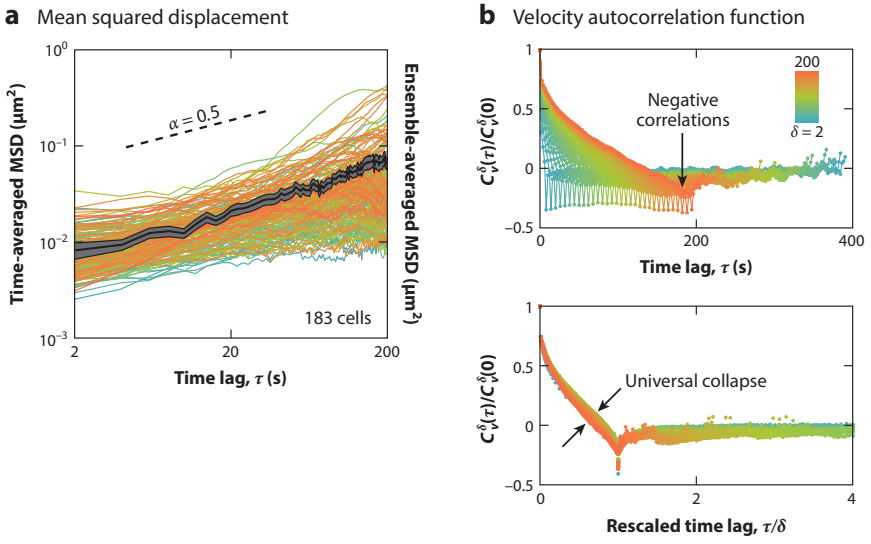

Figure 7

Mean squared displacement (MSD) and velocity autocorrelation function (VAF) as diagnostic tools for DNA motion: an illustration using real DNA trajectories. The data are for D_HJ_H segments in recombination-activating gene–deficient pro-B cells (32). (*a*) Time-averaged MSD (*colored curves*) and ensemble-averaged MSD (*black curve*; shadowed region is the standard error of the mean) as functions of the time lag τ. MSD is calculated from the individual DNA trajectories recorded in 183 cells. On the log-log scale, the slope of MSD yields the scaling exponent α, whereas the y intercept is proportional to the anomalous diffusion coefficient D. Both time- and ensemble-averaged MSD yield similar values of α, a sign of ergodicity. $\alpha \approx 0.5$ indicates that the motion is subdiffusive. (*b*, *top*) VAF curves for different values of the discretization intervals (δ), plotted as a function of the time lag τ. A dip into the negative values indicates the presence of negative correlation. (*b*, *bottom*) VAF curves as a function of the rescaled time lag (τ/δ). A universal collapse is an indication of self-similarity of motion.

self-similarity, or similar patterns at different temporal and spatial scales. Worth noting is that experimental artifacts, such as localization errors or distortions of the trajectories along the z axis resulting from the refractive index mismatch, may affect MSD and VAF and thus should be carefully analyzed (19, 51).

To summarize, the MSD and VAF analysis of the DNA trajectories (**Figure 7**) has revealed that the motion of DNA segments is subdiffusive, ergodic, negatively correlated, and self-similar. How can these properties inform us about the dominant mechanism of motion? Several potentially relevant models, each emphasizing a certain mechanism, are discussed above. We saw that the Rouse model predicts a subdiffusive MSD with $\alpha = 0.5$; however, its picture of the polymer as a noninteracting chain (**Figure 4**) appears to be a poor representation of the crowded nuclear interior (50). Hydrodynamic interactions, which are at the core of the Zimm model (**Figure 4**), have been shown to be largely screened out in an entangled polymer solution (14, 18); it is therefore natural to expect such screening in the crowded nucleus. The reptation model, although explicitly accounting for the entanglement of the polymer solution (**Figure 4**), assumes a particular type of motion in which unstructured polymers are slithering through one another; this picture does not account for the highly structured, hierarchical organization of the chromatin in the nucleus (**Figure 2**). Ergodicity exhibited by DNA trajectories (**Figure 7*a***) suggests that binding-induced pausing events underlying the CTRW model (**Figure 5**), although expected to take place in the

nucleus, do not constitute the dominant factor in the DNA motion (32, 50). Temporal and spatial self-similarity, revealed by the analysis of DNA trajectories (**Figure 7*b***, bottom), is inconsistent with the OD model of diffusion through hard-wall-like obstacles (**Figure 5**), even though this model can indeed lead to negative correlations in the average velocity (32). In contrast, the FLM model of diffusion through a viscoelastic environment (**Figure 5**) possesses all the properties that have been revealed by the trajectories (**Figure 7**): It exhibits ergodicity (16), leads to negative autocorrelations in the velocity, and preserves the self-similarity in space and time (32, 50).

How can we get an intuitive sense of the observed negative correlations in the velocity of DNA segments? Within the picture assumed by the FLM model, negative correlations in velocity are a manifestation of the elastic component (pushback) of the viscoelastic response of the environment. We can try to visualize what is happening: As DNA segments collide with a dense network of nucleic acids and proteins, as well as stretch and compress the neighboring segments of the chromatin fiber, the DNA segments' motion in one direction is likely to be followed by motion in the opposite direction. Mathematically, this reversal in direction for two consecutive steps manifests itself through the fact that correlations in velocity are most negative at $\tau = \delta$ (see **Figure 7**). The viscoelastic mechanism thus emerges as the dominant mechanism governing the motion of DNA segments in the crowded interior of the nucleus. In the corresponding FLM model, Equation 2, the effects of the viscoelastic environment as well as of the polymer nature of DNA itself, including its hierarchical organization, are all packed into the memory kernel and correlated noise terms. This mean-field, or "low-resolution," description means that the many details of DNA motion are accounted for only implicitly. However, the advantage of this description is that it results in a reasonably simple yet general framework, which reveals the general principles underlying genomic encounters and enables us to make testable predictions.

HOW LONG DOES IT TAKE FOR A DNA SEGMENT TO ENCOUNTER ITS DISTANT COUNTERPART? FIRST-PASSAGE TIMES

Having established the dominant mechanism of DNA motion in the nucleus and having mapped this motion onto the corresponding physical model, we are in a position to address the question we posed at the outset: How long does it take for two distant DNA segments to find each other in the crowded interior of the nucleus? In more formal terms, we aim at a general predictive scaling law that would express the mean first-passage time (MFPT) for genomic interaction in terms of the key parameters of the system. Of course, this aim implies that we also need to identify those characteristics that constitute these key parameters.

Thinking about the parameters that might be relevant to the timescale for genomic encounters results in a rather extensive list of candidates: the genomic distance between the segments, their initial physical separation, the distance at which the segments can be considered as interacting, the size of the domain confining the DNA motion, the diffusion coefficient of the segments, and the number of copies of the segments present. To identify the short list, let us first examine a toy version of the original problem—namely, the timescale for the two ends of a chain free in solution to find each other (i.e., to form a loop). Intuitively, one expects that the two ends are more likely to encounter each other when the distance between them along the chain (the contour length) is shorter, the interaction distance is larger, and their diffusion coefficient is higher (38). However, in the context of our original problem—that of the encounters between remote DNA segments in a crowded nucleus—such expectations need to be revisited. First, due to the multilevel folding of chromatin into loops, loop bundles, and domains, remote DNA segments may "not be aware" of the fact that they belong to the same chain, and their initial physical separation may no longer be dictated by their genomic distance. Rather, the size of the domain acting as the

confinement becomes the likely determinant of both the initial and average separations between the segments. Second, recall that the viscoelastic environment of the nucleus makes the motion of the DNA segments strongly subdiffusive (**Figure 7**). For strongly subdiffusive motion, the interaction distance r_0 has been shown to be a second-order effect in the MFPT due to the tendency of such motion to retrace previously visited areas, the phenomenon known as compact exploration (4, 11, 41). Taken together, the above arguments suggest that the encounter timescale for remote DNA segments in the nucleus should be determined mainly by the radius of confinement R (set by the size of the genetic loci), the subdiffusive scaling exponent α, and the anomalous diffusion coefficient D.

These arguments can be made more precise with a simple dimensional analysis (32). The dimensions of MSD are $[\text{MSD}] = [\text{length}]^2 = [D]\,[\text{Time}]^\alpha$ (we use the standard notation of brackets to represent the dimension of the quantity within the brackets), which gives $[\text{Time}] = [\text{length}]^{2/\alpha}\,[D]^{-1/\alpha}$. As we just discussed, the relevant parameter with the dimensions of length in our first-passage time problem is the radius of confinement R. Thus, MFPT scales with the confinement radius as $R^{2/\alpha}$ and with the diffusion coefficient as $D^{-1/\alpha}$. Interesting to note is that the results of our dimensional analysis are in agreement with the corresponding results in the narrow-window escape time problems (4, 11). Finally, one more factor to consider is that a genomic interaction may involve a DNA segment that is available in multiple copies. This, for example, is the case in somatic recombination underlying the production of the diverse repertoire of antibodies (1). When the encounter is a rare event (which seems reasonable to assume for remote DNA encounters), it is natural to expect that the encounter probability, and, consequently, the inverse of the MFPT, should be proportional to the number of segment copies, N. Summarizing the above arguments, we arrive at the scaling relationship for the MFPT for remote genomic encounters in terms of the key parameters:

$$\text{MFPT} \propto N^{-1} R^{2/\alpha} D^{-1/\alpha}. \qquad 4.$$

With the analytical relationship in Equation 4, we are now in a position to make concrete, testable predictions. Substituting the value of $\alpha = 1/2$ extracted from the experimental measurements (**Figure 7**), we find from Equation 4 that a 2-fold decrease in the radius of confinement would yield a 16-fold decrease in the MFPT. With 100 copies of the DNA segment present, the MFPT is predicted by Equation 4 to decrease 100-fold compared with that for a single pair of segments. Note that the $R^{2/\alpha}$ dependence of the MFPT is rather strong when the motion is subdiffusive: With $\alpha = 1/2$, the scaling becomes $\text{MFPT} \propto R^4$, and the confinement emerges as an important factor for achieving short encounter times for remote DNA segments (32).

A useful tool for validating our analytical scaling law (Equation 4) is provided by numerical simulations. With a model and the corresponding mathematical description (Equation 2) in hand, and with input parameters from experimental data (**Figure 7**), we are justified in our hopes that such simulations, although not replete with details, are reasonably realistic in approximating genomic encounters in live cells. The problem of first-passage times for two genomic elements can be simulated as the anomalous diffusion of two particles in a confinement of radius R (**Figure 8**). On the basis of the observation that genomic interactions occur mainly within the same topological domain (17, 30, 31), it is natural to interpret the confinement in the simulations as one such domain (**Figure 2**). The motion of the particles representing the DNA segments is governed by the fractional Langevin equation, Equation 2, or, more specifically, by its simplified version corresponding to the high friction situation. In this so-called overdamped limit, the inertia term $m\frac{d^2\mathbf{R}}{dt^2}$ in Equation 2 is neglected on the basis that, in the limit of large γ, the timescale at which the velocity equilibrates, m/γ, is shorter than any other characteristic timescale of the system (37). The effect of the confinement can be incorporated in the overdamped fractional Langevin

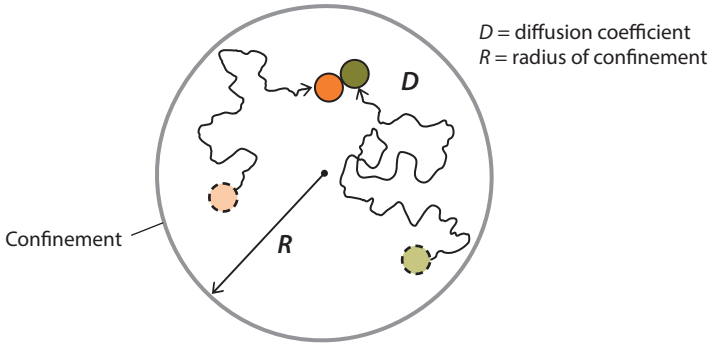

Figure 8

The problem of first-passage times for two genomic elements can be simulated as the anomalous diffusion of two particles in a confinement of radius R (representing a chromosomal domain; see **Figure 2**) with the anomalous diffusion coefficient D. The motion of the particles is governed by the fractional Langevin equation, Equation 2.

equation through the external force $\boldsymbol{F}$ either as a reflective force from the boundary (23) or as a restoring force from a harmonic potential confining the motion (24, 26). Once the two particles (segments) are within the interaction distance r_0, the corresponding first-passage time is recorded. The values of the scaling exponent α and the anomalous diffusion coefficient D (the latter is inversely proportional to the friction coefficient γ) can be extracted from the MSD of the experimental data (**Figure 7**) and used as input in the simulations. The natural choice of the interaction distance is the thickness of the chromatin fiber, $r_0 = 30$ nm (1), and the radius of confinement is dictated by the typical size of a domain, on the order of a micrometer (25, 54).

Figure 9 shows some of the outcomes of the simulations, which directly test the predictions of Equation 4 regarding the MFPT. The MFPT for two DNA segments in a confinement of radius

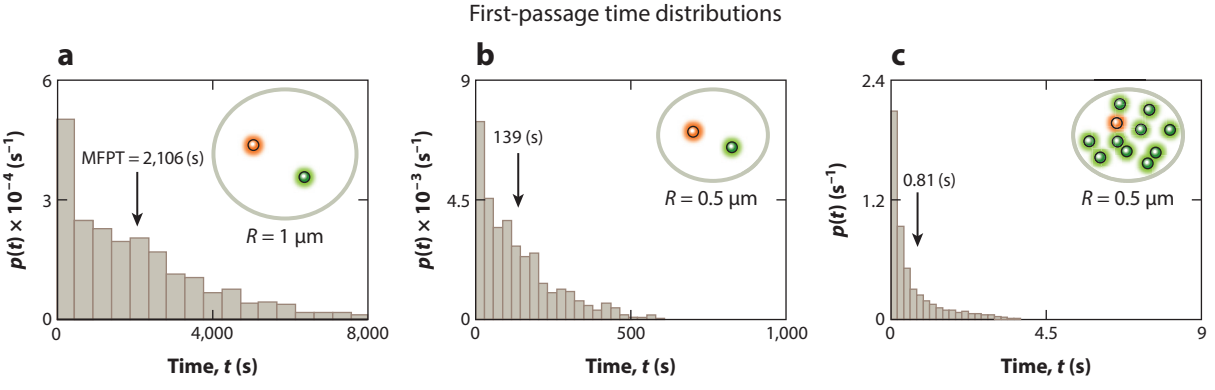

Figure 9

Distributions of the first-passage times obtained from the simulations of distant DNA segments undergoing fractional Langevin motion in a confining sphere of radius R. (*a*) A single pair of DNA segments diffusing in a spatial confinement of radius 1 μm and with initial positions randomly chosen from the equilibrium distribution. The arrow indicates the mean first-passage time (MFPT). (*b*) Simulation as performed in panel *a* but with a confinement of radius 0.5 μm. Note that decreasing the confinement size by a factor of 2 accelerates the first-passage time by a factor of 16, in agreement with the prediction in Equation 4. (*c*) Simulation as performed in panel *b* but with 100 copies of one of the DNA segments. Note that the MFPT decreases by approximately a factor of 100, in accord with the prediction by Equation 4. Figure adapted from Reference 32 with permission.

$R = 1$ μm is about 30 min (**Figure 9*a***). When the confinement radius is reduced by half, the MFPT is only approximately 2 min (**Figure 9*b***), in agreement with the 16-fold decrease predicted by Equation 4. When one of the DNA segments is present in 100 copies, the MFPT decreases further to just approximately a second (**Figure 9*c***), confirming that the prediction of the 100-fold decrease by Equation 4 is quite accurate.

OUTLOOK

The question we asked at the outset concerned two DNA segments faced with the task of finding each other in the crowded nucleus. We saw that however improbable it may seem to fulfill this task on a short timescale, the cell can accomplish it by utilizing a basic physical mechanism of motion—which is likely to be universal across species—without the need to rely on sophisticated regulation mechanisms. However, genomic interactions are inherently a many-body problem: Productive genomic contacts may not only involve more than two genomic segments but may also involve a suite of regulating proteins. The outcome in which all these components quickly end up, by mere chance, in the same location at the same time may seem extremely unlikely. Then, how exactly does increasing the number of required participants affect the first-passage times for genomic encounters? Scaling relationships, of the sort that would generalize Equation 4, would not only provide the answer but also reveal the general principles behind the many-body version of this first-passage time problem.

An important aspect of genomic interactions that we emphasized in this review is the intimate connection between the architecture of the genome and its motion. This connection inspires the idea of building a comprehensive, yet conceptually distilled, four-dimensional picture of the genome—that is, of its structural and functional organization in both space and time. Fortunately, experimental research is advancing rapidly on both fronts: Single-molecule tracking experiments are visualizing, in increasingly more detail, the real-time motion of DNA, while high-throughput structural methods such as Hi-C are revealing new patterns of the genome structure. Merging the dynamic and structural information into a unified, tractable spatiotemporal picture of the genome is an exciting challenge at the interface of biology and physics.

As technologies move forward, visualizing genomic events in great detail should soon be possible—for example, simultaneously observing the motion and interactions of multiple genomic segments within the same chromosomal neighborhood. However, the vast amount of new data will come with a challenge: To make sense of such detailed data will require a description that is realistic yet transcends the details of particular systems—the type of description that has become the standard in physics (5). How can we construct such a description? Observations of genomic interactions in individual biological systems will hopefully provide glimpses of deep and unifying principles that operate across all these systems. Recognizing these general principles and casting them into a unifying mathematical framework will, in return, enable concrete predictions for particular systems.

Remote chromosomal interactions are at the core of a broad range of essential processes in biology, yet even basic questions still need to be addressed. Due to emerging technologies and increasingly sophisticated experiments, the vast subject of genomic interactions is now ripe for quantitative approaches from physics. The interplay between quantitative biological experimentation and conceptually simplified models that are at the heart of physics is, in our view, an exciting and fruitful route to revealing the unifying principles behind the extraordinary complexity of the processes in the genome.

DISCLOSURE STATEMENT

The authors are not aware of any affiliations, memberships, funding, or financial holdings that might be perceived as affecting the objectivity of this review.

ACKNOWLEDGMENTS

We thank Kees Murre, Alex Groisman, and Christopher Pierse for valuable comments on the manuscript. Support was provided by the National Science Foundation grant No. MCB-1411884.

LITERATURE CITED

1. Alberts B, Johnson A, Lewis J, Raff M, Roberts K, Walter P. 2007. *Molecular Biology of the Cell*. New York: Garland Sci. 5th ed.
2. Ariel F, Jegu T, Latrasse D, Romero-Barrios N, Christ A, et al. 2014. Noncoding transcription by alternative RNA polymerases dynamically regulates an auxin-driven chromatin loop. *Mol. Cell* 55:383–96
3. ben-Avraham D, Havlin S. 2000. *Diffusion and Reactions in Fractals and Disordered Systems*. Cambridge, UK: Cambridge Univ. Press
4. Bénichou O, Voituriez R. 2008. Narrow-escape time problem: time needed for a particle to exit a confining domain through a small window. *Phys. Rev. Lett.* 100:168105
5. Bialek W. 2012. *Biophysics: Searching for Principles*. Princeton, NJ: Princeton Univ. Press
6. Bickmore WA, van Steensel B. 2013. Genome architecture: domain organization of interphase chromosomes. *Cell* 152:1270–84
7. Blackwood EM, Kadonaga JT. 1998. Going the distance: a current view of enhancer action. *Science* 281:60–63
8. Bohn M, Heermann DW. 2010. Diffusion-driven looping provides a consistent framework for chromatin organization. *PLOS ONE* 5(8):e12218
9. Bronstein I, Israel Y, Kepten E, Mai S, Shav-Tal Y, et al. 2009. Transient anomalous diffusion of telomeres in the nucleus of mammalian cells. *Phys. Rev. Lett.* 103:018102
10. Cabal GG, Genovesio A, Rodriguez-Navarro S, Zimmer C, Gadal O, et al. 2006. SAGA interacting factors confine sub-diffusion of transcribed genes to the nuclear envelope. *Nature* 441:770–73
11. Condamin S, Bénichou O, Tejedor V, Voituriez R, Klafter J. 2007. First-passage times in complex scale-invariant media. *Nature* 450:77–80
12. Cremer T, Cremer C. 2001. Chromosome territories, nuclear architecture and gene regulation in mammalian cells. *Nat. Rev. Genet.* 2:292–301
13. Croft JA, Bridger JM, Boyle S, Perry P, Teague P, Bickmore WA. 1999. Differences in the localization and morphology of chromosomes in the human nucleus. *J. Cell Biol.* 145:1119–31
14. de Gennes PG. 1971. Reptation of a polymer chain in the presence of fixed obstacles. *J. Chem. Phys.* 55:572–79
15. Dekker J, Rippe K, Dekker M, Kleckner N. 2002. Capturing chromosome conformation. *Science* 295: 1206–11
16. Deng W, Barkai E. 2009. Ergodic properties of fractional Brownian-Langevin motion. *Phys. Rev. E* 79:011112
17. Dixon JR, Selvaraj S, Yue F, Kim A, Li Y, et al. 2012. Topological domains in mammalian genomes identified by analysis of chromatin interactions. *Nature* 485:376–80
18. Doi M, Edwards SF. 1986. *The Theory of Polymer Dynamics*. New York: Oxford Univ. Press
19. Ferko MC, Patterson BW, Butler PJ. 2006. High-resolution solid modeling of biological samples imaged with 3D fluorescence microscopy. *Microsc. Res. Tech.* 69:648–55
20. Fisher JK, Bourniquel A, Witz G, Weiner B, Prentiss M, Kleckner N. 2013. Four-dimensional imaging of *E. coli* nucleoid organization and dynamics in living cells. *Cell* 153:882–95
21. Grunstein M. 1997. Histone acetylation in chromatin structure and transcription. *Nature* 389:349–52

22. He Y, Burov S, Metzler R, Barkai E. 2008. Random time-scale invariant diffusion and transport coefficients. *Phys. Rev. Lett.* 101:058101
23. Jeon JH, Metzler R. 2010. Fractional Brownian motion and motion governed by the fractional Langevin equation in confined geometries. *Phys. Rev. E* 81:021103
24. Jeon JH, Metzler R. 2012. Inequivalence of time and ensemble averages in ergodic systems: exponential versus power-law relaxation in confinement. *Phys. Rev. E* 85:021147
25. Jhunjhunwala S, van Zelm MC, Peak MM, Cutchin S, Riblet R, et al. 2008. The 3D structure of the immunoglobulin heavy-chain locus: implications for long-range genomic interactions. *Cell* 133:265–79
26. Kou SC, Xie XS. 2004. Generalized Langevin equation with fractional Gaussian noise: subdiffusion within a single protein molecule. *Phys. Rev. Lett.* 93:180603
27. Krivega I, Dean A. 2012. Enhancer and promoter interactions—long distance calls. *Curr. Opin. Genet. Dev.* 22:79–85
28. Lamond AI, Earnshaw WC. 1998. Structure and function in the nucleus. *Science* 280:547–53
29. Langevin P. 1908. Sur la théorie du mouvement brownien [On the theory of Brownian motion]. *C. R. Acad. Sci. (Paris)* 146:530–33
30. Lieberman-Aiden E, van Berkum NL, Williams L, Imakaev M, Ragoczy T, et al. 2009. Comprehensive mapping of long-range interactions reveals folding principles of the human genome. *Science* 326:289–93
31. Lin YC, Benner C, Mansson R, Heinz S, Miyazaki K, et al. 2012. Global changes in the nuclear positioning of genes and intra- and interdomain genomic interactions that orchestrate B cell fate. *Nat. Immunol.* 13:1196–204
32. Lucas JS, Zhang Y, Dudko OK, Murre C. 2014. 3D trajectories adopted by coding and regulatory DNA elements: first-passage times for genomic interactions. *Cell* 158:339–52
33. Lutz E. 2001. Fractional Langevin equation. *Phys. Rev. E* 64:051106
34. Metzler R, Klafter J. 2000. The random walk's guide to anomalous diffusion: a fractional dynamics approach. *Phys. Rep.* 339(1):1–77
35. Montroll EW, Weiss GH. 1965. Random walks on lattices. II. *J. Math. Phys.* 6:167–81
36. Niki H, Yamaichi Y, Hiraga S. 2000. Dynamic organization of chromosomal DNA in *Escherichia coli*. *Genes Dev.* 14:212–23
37. Nitzan A. 2006. *Chemical Dynamics in Condensed Phases: Relaxation, Transfer, and Reactions in Condensed Molecular Systems*. New York: Oxford Univ. Press
38. Pastor RW, Zwanzig R, Szabo A. 1996. Diffusion limited first contact of the ends of a polymer: comparison of theory with simulation. *J. Chem. Phys.* 105:3878–82
39. Phillips R, Kondev J, Theriot J, Garcia HG. 2012. *Physical Biology of the Cell*. London/New York: Garland Sci. 2nd ed.
40. Qian H. 2003. Fractional Brownian motion and fractional Gaussian noise. In *Processes with Long-Range Correlations: Theory and Applications*, ed. G Rangarajan, M Ding, pp. 22–33. New York: Springer
41. Redner S. 2001. *A Guide to First-Passage Processes*. Cambridge, UK: Cambridge Univ. Press
42. Rouse PE. 1953. A theory of the linear viscoelastic properties of dilute solutions of coiling polymers. *J. Chem. Phys.* 21:1272–80
43. Saxton MJ. 1994. Anomalous diffusion due to obstacles: a Monte Carlo study. *Biophys. J.* 66:394–401
44. Saxton MJ. 1996. Anomalous diffusion due to binding: a Monte Carlo study. *Biophys. J.* 70:1250–62
45. Spector DL. 2003. The dynamics of chromosome organization and gene regulation. *Annu. Rev. Biochem.* 72:573–608
46. Splinter E, Heath H, Kooren J, Palstra RJ, Klous P, et al. 2006. CTCF mediates long-range chromatin looping and local histone modification in the β-globin locus. *Genes Dev.* 20:2349–54
47. Thanbichler M, Wang SC, Shapiro L. 2005. The bacterial nucleoid: a highly organized and dynamic structure. *J. Cell. Biochem.* 96:506–21
48. Tonegawa S. 1983. Somatic generation of antibody diversity. *Nature* 302:575–81
49. Vazquez J, Belmont AS, Sedat JW. 2001. Multiple regimes of constrained chromosome motion are regulated in the interphase *Drosophila* nucleus. *Curr. Biol.* 11:1227–39
50. Weber SC, Spakowitz AJ, Theriot JA. 2010. Bacterial chromosomal loci move subdiffusively through a viscoelastic cytoplasm. *Phys. Rev. Lett.* 104:238102

51. Weber SC, Thompson MA, Moerner WE, Spakowitz AJ, Theriot JA. 2012. Analytical tools to distinguish the effects of localization error, confinement, and medium elasticity on the velocity autocorrelation function. *Biophys. J.* 102:2443–50
52. Woodcock CL, Ghosh RP. 2010. Chromatin higher-order structure and dynamics. *Cold Spring Harb. Perspect. Biol.* 2:a000596
53. Zimm BH. 1956. Dynamics of polymer molecules in dilute solution: viscoelasticity, flow birefringence and dielectric loss. *J. Chem. Phys.* 24:269–78
54. Zink D, Cremer T, Saffrich R, Fischer R, Trendelenburg MF, et al. 1998. Structure and dynamics of human interphase chromosome territories in vivo. *Hum. Genet.* 102:241–51

Annual Review of Biophysics
Volume 45, 2016

Contents

Indexes

Errata

An online log of corrections to *Annual Review of Biophysics* articles may be found at http://www.annualreviews.org/errata/biophys